New insights in the leaching kinetics of cathodic materials in acidic chloride media for lithium-ion battery recycling

Wen Xuan, Antônio de Souza Braga, Chloé Korbel, Alexandre Chagnes

New insights in the leaching kinetics of cathodic materials in acidic chloride media for lithium-ion battery recycling

Wen Xuan[a], Antônio Braga de Souza[a], Chloé Korbel[a], Alexandre Chagnes[a]*

[a] *Université de Lorraine, CNRS, GeoRessources, F- 54000 Nancy, France.*

Abstract

Leaching reactions in hydrochloric acid of several cathodic materials used in lithium-ion batteries were investigated between 25 °C and 82 °C. The dissolution rate increased as follows: NMC811 ($LiNi_{0.8}Mn_{0.1}Co_{0.1}O_2$) > NMC622 ($LiNi_{0.6}Mn_{0.2}Co_{0.2}O_2$) >> NMC532 ($LiNi_{0.5}Mn_{0.3}Co_{0.2}O_2$) > NMC111 ($LiNi_{1/3}Mn_{1/3}Co_{1/3}O_2$). The dissolution of lithium is faster than that for nickel, cobalt and manganese. Data analysis demonstrated that NMC dissolution is always a two-step process. In the first step, NMC was transformed very quickly into a new lithium-defficient phase. This phase was subsequently dissolved during a second-rate limiting step. No significant impact of the solid/liquid ratio on the leaching kinetics was observed as far as the solid-liquid ratio remained below the stochiometric composition. Finally, a shrinking core model and a first-order rate law were used to investigate the leaching kinetics of the second rate-limiting step, which is the main step involved during NMC digestion in hydrochloric acid.

Keywords: Lithium-ion batteries, NMC, hydrochloric acid, leaching, kinetics, recycling.

*Correspondence should be addressed to:
Alexandre Chagnes (alexandre.chagnes@univ-lorraine.fr)

1. Introduction

Lithium-ion batteries (LIBs) are composed of cathode, anode and electrolyte, which contain valuable metals. Among the main cathodes reported in the last decades (**Table 1**), lithiated nickel-manganese-cobalt oxide electrodes abbreviated as NMC ($LiNi_{1-x-y}Mn_xCo_yO_2$) are the most widely used material in LIBs. The electrochemical and physicochemical properties of NMC electrodes depend on their compositions (Gong et al. 2017): (i) high nickel content is responsible for high capacity and high charge-discharge rate at the expense of poor safety, (ii) high manganese content improves the safety and increases the lifespan of the electrode, and (iii) high cobalt content stabilizes the NMC layer structure and improves the charge-discharge rate. Four types of NMC cathodes containing nickel, cobalt, manganese and lithium are available to satisfy the needs in terms of stability, charge-discharge rate, cycle ability and capacity: NMC811 ($LiNi_{0.8}Mn_{0.1}Co_{0.1}O_2$), NMC622 ($LiNi_{0.6}Mn_{0.2}Co_{0.2}O_2$), NMC532 ($LiNi_{0.5}Mn_{0.3}Co_{0.2}O_2$) and NMC111 ($LiNi_{1/3}Mn_{1/3}Co_{1/3}O_2$).

Therefore, the huge increase in electric vehicle production in the next decade will impact the future demand of cobalt, nickel and lithium, which will likely increase by 31%, 69% and 46% between 2017 and 2030, respectively (Chagnes, 2019, Chagnes and Pospiech, 2013). Recycling appears in part as one of the solutions to face up this demand (Pagliaro and Meneguzzo, 2019). Furthermore, the environmental footprint of raw material production can be significantly reduced by processing spent materials rather than primary resources due to the high environmental impact of mining, comminution and ore beneficiation. For instance, the production of transition metals, generally extracted from sulfide ores, contributes dramatically to SOx emissions, which are drastically reduced by implementing recycling processes. More generally, the closer the recycled material is to its final product, the more the net production impacts can be reduced (Gaines, 2018).

In order to face up cobalt, nickel, manganese and lithium demand due to the emergence of electric vehicle, the developpement of recycling processes of spent LIBs is challenging (Pagliaro and Meneguzzo, 2019). In particular, many efforts concern the recovery of lithium, cobalt, nickel and manganese from the $LiNi_{1-x-y}Mn_xCo_yO_2$ cathodic material. Although, several studies addressed leaching of NMC111 ($LiNi_{1/3}Mn_{1/3}Co_{1/3}O_2$), LCO ($LiCoO_2$), LMO ($LiMnO_2$), LNO ($LiNiO_2$) and LFP ($LiFePO_4$), only few studies investigated the leaching mechanisms of NMC811, NMC622, and NMC532 in spite of their potential uses as new cathodes (**Table 1**).

Hydrometallurgy appears to be the best technology to extract and separate metals from spent LIBs (Boyden et al., 2016). Hydrochloric acid, nitric acid, sulfuric acid and several organic acids such as lactic acid, citric acid, formic acid, and tartaric acid were tested in previous works to leach cathodic materials (Ordoñez et al., 2016). Likewise, several studies addressed the use of hydrochloric acid in order to take advantage of its reactivity and the formation of metal chloride species in solution, which may improve the selectivity of the liquid-liquid extraction stage usually implemented to extract and separate metals contained in the leachate (Seeley and Crouse, 1966; Zhu et al., 2017). This paper investigates the leaching kinetics of NMC811, NMC622, NMC532 and NMC111 in hydrochloric acid. Kinetic data were analyzed by means of two models that fairly describe the digestion of NMC cathodic materials in acidic chloride media.

2. Material and methods

Hydrochloric acid (37% weight) was supplied by Sigma Aldrich. The battery materials NMC811, NMC622, NMC532 and NMC111 were supplied by Xiamen Tob New Technology Co., LTD. The particle size distribution is reported in **Figure 1**. The leaching experiments were performed between 25 °C and 82 °C in a homemade double-jacketed 1L-glassware reactor thermostated with a Lauda thermostat (**Figure 2**). Diluted acid was added into the reactor under agitation before introducing the cathodic material (powder). Samples were withdrawn regularly from the reactor and immediately filtered.

Nickel, cobalt, manganese and lithium concentrations were analysed by Microwave Plasma-Atomic Emission Spectrometry with appropriate standards (Agilent 4210 MP-AES).

The leaching efficiency of the chemical element i was calculated by using the following equation deduced from the mass-balance:

$$\%\boldsymbol{E_i} = \frac{\boldsymbol{C_f(i) - C_0(i)}}{\boldsymbol{Cf(i)}} \times \mathbf{100}\% \quad (1)$$

where $C_f(i)$ and $C_0(i)$ are the final and initial concentrations of the metal i in the leach solution, respectively. The metal concentrations in the residues during leaching and the metal concentrations in the leach solution after full digestion of the cathodic materials were used to recalculate the cathode composition and check the mass-balance.

Table 3 shows a comparison of this result with the theoretical liquor composition. This calculation confirmed the validity of **Eq (1)**.

Chloride concentrations in the samples were determined by ion chromatography (ICS-900 Dionex) equipped with the column IC Dionex™ IonPac™ AS22.

3. Results and Discussions

Wang et al. (2009) showed that it was possible to achieve a full dissolution of cobalt, manganese, nickel and lithium from $LiCoO_2$, $LiMn_2O_4$ or $LiNi_{1/3}Mn_{1/3}Co_{1/3}O_2$ by using hydrochloric acid. In the case of $LiCoO_2$, it is usually stated that the leaching mechanism by HCl can be described by the following equation (Takacova et al., 2016):

$$\mathbf{2LiCoO_{2,(s)} + 8HCl_{(l)} \rightleftharpoons 2LiCl_{(l)} + 2CoCl_{2,(l)} + 4H_2O_{(l)} + Cl_{2,(g)}} \quad (2)$$

In the present study, leaching experiments of NMC532, NMC811 and NMC622 were performed under similar experimental conditions as those reported by Wang et al. (2009) but at different leaching temperatures, i.e. a solid/liquid phase ratio of S/L=20 g/L, an hydrochloric acid concentration of 4 mol L^{-1} and temperatures ranging form 25 °C to 82 °C.

Figure 3 shows the influence of the temperature on the dissolution of nickel, cobalt, manganese and lithium from NMC811 as a function of time. The leaching kinetics of the other NMC cathodic materials are reported in the Supporting Information (**Figures S1-S16**). The NMC materials were fully dissolved under these experimental conditions. No significant difference in the dissolution kinetics was observed for nickel, manganese and cobalt. Conversely, the dissolution kinetics of lithium from all cathodic materials were much faster than those obtained for nickel, manganese and cobalt. Furthermore, it was observed that the digestion of the cathodic materials containing high content of nickel or low content of manganese was faster (NMC811 and NMC622). The comparison of the leaching curves reported in **Figure 3** and **Figures S1-S16** (Supporting Information) leads to the conclusion that the leaching kinetics follows this order: NMC811 > NMC622 >> NMC532 > NMC111 at 54 °C. It is in accordance with the stability of the NMC electrodes, which is higher for manganese-rich cathodes (Gong et al., 2017).

3.1 Kinetic models

3.1.1 Empirical model based on chloride consumption

In our previous paper (Xuan et al., 2019), it was demonstrated that NMC111 digestion involves the two following steps:

Step 1:

$$LiMO_{2,(s)} + \frac{4n-4}{2n-1}HCl_{(l)} \rightleftharpoons \frac{2n-2}{2n-1}LiCl_{(l)} + \frac{n-1}{2n-1}MCl_{2,(l)} + \frac{n}{2n-1}Li_{\frac{1}{n}}MO_{2,(s)} + \frac{2n-2}{2n-1}H_2O_{(l)} \quad (3)$$

Step 2: (rate limiting reaction)

$$Li_{\frac{1}{n}}MO_{2,(s)} + 4HCl_{(l)} \rightleftharpoons \frac{1}{n}LiCl_{(l)} + MCl_{2,(l)} + 2H_2O_{(l)} + \left(1-\frac{1}{2n}\right)Cl_{2,(g)} \quad (4)$$

The overall equation can be written as:

$$2LiMO_{2,(s)} + 8HCl_{(l)} \rightleftharpoons 2LiCl_{(l)} + 2MCl_{2,(l)} + 4H_2O_{(l)} + Cl_{2,(g)} \quad (5)$$

where the first step results in the formation of an intermediate product $Li_{\frac{1}{n}}MO_{2,(s)}$ with M=Ni, Mn or Co. The parameter n denotes the molar ratio between all transition metals and lithium in the intermediate product, which was calculated by plotting the total concentration of nickel, manganese and cobalt as a function of lithium concentration in the leachate (Xuan et al., 2019). The values of n were found to range from 2.1 to 4.0 when the solid/liquid ratio (S/L) and the temperatures were comprised between 20 and 80 g/L, and between 25 and 82 °C, respectively (**Table 4**).

Release of chlorine gas was observed during the NMC digestion due to chloride oxidation (Eq (4)). The chloride concentration in the leach solution can be calculated as a function of the leaching time by using the following semi-empirical equation when the step 2 is predominant:

$$[Cl^-]_t = ([Cl^-]_\infty - [Cl^-]_O)[1 - exp(-at)] + [Cl^-]_O \quad (6)$$

where $[Cl^-]_0$, $[Cl^-]_t$, and $[Cl^-]_\infty$ denote the chloride concentration in the leach solution at the begining of the experiment, at time t and at infinite time, respectively. In this equation, the initial chloride concentration corresponds to the initial concentration of hydrochloric acid and the theoretical value of the chloride concentration at infinite time can be deduced by the following equation:

$$[Cl^-]_\infty = [Cl^-]_O - \frac{1}{M_{NMC}}\left(\frac{S}{L}\right) \quad (7)$$

where M_{NMC} (in g/mol) is the molecular weight of NMC and S/L (in g/L) is the solid/liquid phase ratio. The chloride concentration at infinite time $[Cl^-]_\infty$ is equal to 3.8 mol L^{-1} and 3.2 mol L^{-1} when 4.0 mol L^{-1} HCl is used to leach the NMC materials at S/L=20 g/L and 80 g/L, respectively.

Figure 4 shows the variation of the chloride concentration as a function of time when NMC532 was leached in 4 mol L^{-1} HCl at 82 °C and S/L= 20 g/L. There is a fair agreement between the experimental data and those calculated by using the semi-empirical **Eq (6)**.

To assess the relative success of the semi-empirical model applied to various experimental conditions (**Figures S17-S27**), a linear square regression analysis of the form:

$$[Cl-]_{t,exp} = u\,[Cl-]_{t,calc} \quad (8)$$

was employed where $[Cl^-]_{t,calc}$ and $[Cl^-]_{t,exp}$ represent the calculated and experimental values of the chloride concentration in the leach solution at time t, respectively; u is the conversion factor.

Eq (6) describes fairly the experimental data as the values of u deduced from Eq. (8) and the standard deviation R^2 of Eq. (8) are close to the unity (**Table 5**). The theoritical values of $[Cl^-]_\infty$ are in agreement with those calculated by Eq (7): $[Cl^-]_\infty$=3.7-3.9 mol L^{-1} at S/L=20 g/L and $[Cl^-]_\infty$=3.2-3.3 mol L^{-1} at S/L=80 g/L, whereas the theoretical values are equal to 3.8 and 3.2 mol·L^{-1}, respectively (**Table 5**).

The following equations can be written by using Eqs (3)-(4) and Eq (6):

$$[Li] = \frac{1}{M_{NMC}}\left(\frac{2n-2}{2n-1}\right)\frac{S}{L} + \frac{([Cl^-]_\infty - [Cl^-]_O)[1-exp(-at)]+[Cl^-]_O}{2n-1} \quad (9)$$

$$[Ni]+[Mn]+[Co] = \frac{1}{M_{NMC}}\left(\frac{n-1}{2n-1}\right)\frac{S}{L} + \frac{([Cl^-]_\infty - [Cl^-]_O)[1-exp(-at)]+[Cl^-]_O}{2-\frac{1}{n}} \quad (10)$$

where M_{NMC} (in g/mol) is the molar mass of NMC corresponding to 1 mol of Li and $\frac{S}{L}$ (in g/L) is the solid/liquid phase ratio.

Eqs (9) and (10) were used to calulate the metal concentration as a function of the leaching time. For the sake of illustration, the comparison of the experimental data and the calculated values are displayed in **Figure 5** for NMC532 digested in 4 mol L^{-1} HCl at 82 °C. The other results are available in the Supporting Information.

It is interesting to highlight that lithium dissolution was faster than that observed for nickel, cobalt and manganese at the beginning of the reaction. This difference in kinetic behavior might be explained by the fact that the mechanism of lithium dissolution does not involve any reduction [**Eqs (3) and (4)**] unlike cobalt, nickel and manganese (Buzatu et al., 2014).

The leaching of NMC811 was tested in 4 mol L^{-1} at 25 °C and three different S/L ratios, i.e. 2 g/L, 20 g/L and 80 g/L. According to **Eq (5)**, 4 mol L^{-1} HCl cannot dissolve more than 97.3 g/L NMC811. Below this stochiometric limit, the leaching kinetics of Li, Co, Ni and Mn hardly depend on the S/L ratio (**Figure 6**).

Eqs (9) and (10) can also be used to investigate the effect of S/L ratios on the leaching kinetics. **Figure 7** shows the variation of the lithium concentration and the variation of the total concentrations of cobalt, nickel and manganese as a function of the leaching time at two different S/L ratios, i.e. 80 g/L for NMC111 at 25 °C, and 20 g/L for NMC 622 at 54 °C. These experimental results are in fair agreement with **Eqs (9) and (10)**. Therefore, the present model can fairly predict the leaching kinetics as a function of S/L ratios. Additional results are available in the Supporting Information (**Figures S28-S38**).

Figure 8 confirms that **Eqs (9) and (10)** can be used to calculate the concentrations of cobalt, nickel, manganese and lithium in the leachate at any S/L ratios for the four NMC cathodic materials.

3.1.2 First-order rate law

The first-order rate law was used to describe the rate of many chemical systems in the literature. This law was used in the present paper to describe the rate of NMC digestion in HCl media.

The following equation can be written:

$$[Ni]' + [Mn]' + [Co]' = n[Li]' = \frac{[HCl]_0 - [HCl]}{4} = f(t') \quad (11)$$

where [Ni]', [Mn]', [Co]' and [Li]' represent nickel, cobalt, manganese and lithium concentrations dissolved in the leach solution during the second step, respectively. The term $[HCl]_0$ is the acid concentration at the end of the first step and the term [HCl] denotes the acid concentration at time t' (where t' is the time during the second step, which is the difference between the total time t and the transition time t_0 when the first step finishes).

$$t' = t - t_0 \quad (12)$$

The transition time t_0 can be determined by using the approach below. According to **Eq (3)**, the following mass-balance equations can be written for step 1 and step 2, respectively:

$$[Ni] + [Mn] + [Co] = \frac{1}{2}[Li] \quad (13)$$

$$[Ni] + [Mn] + [Co] = n[Li] + b \quad (14)$$

where n is defined in **Eq (4)**, and b is an empirical constant. Both n and b can be determined by plotting [Ni]+[Mn]+[Co] with [Li].

These two equations are equal at the transition times corresponding to the end of the first step and the beginning of the second step. Therefore, the sum of the concentrations of cobalt, nickel and manganese as well as the lithium concentration in the leach solution at the transition point can be calculated by using the following equations deduced from **Eqs (15) and (16)**:

$$[Li]_0 = \frac{2b}{1-2n} \quad (15)$$

$$[Ni]_0 + [Mn]_0 + [Co]_0 = \frac{b}{1-2n} \quad (16)$$

Figure 9 illustrates the way to determine the transition concentrations for NMC111 leached in 4 mol L^{-1} HCl at 54 °C. The intersection of the two straight lines corresponds to the concentrations of lithium ($[Li]_0$), and the sum of the concentrations of nickel, cobalt and manganese in the leach solution ($[Ni]_0+[Mn]_0+[Co]_0$) at the transition time.

The transition time (t_0) can be deduced by using the following empirical equations given that the values of $[Ni]_0 + [Mn]_0 + [Co]_0$ were previously determined by using the following relatioship:

$$[Ni]_0 + [Mn]_0 + [Co]_0 = \left(\frac{1}{M_{NMC}}\frac{S}{L} - [Ni]_0 - [Mn]_0 - [Co]_0\right)[1 - e^{(-k_1 t_0 + f)}] \quad (17a)$$

In this equation, $\left(\frac{1}{M_{NMC}}\frac{S}{L} - [Ni]_0 - [Mn]_0 - [Co]_0\right)$ is the theoretical maximum sum of the concentrations of Ni, Mn and Co when all the solid is dissolved, which is calculated by the total number of moles of Ni, Mn and Co from the solid subtracted by the dissolved part during the first step. The constants k_1 and f have been deduced by fiting the experimental data of metal dissolution vs. time with the following general equation used to describe NMC digestion, using solve of Excel:

$$[Ni]' + [Mn]' + [Co]' = \left(\frac{1}{M_{NMC}}\frac{S}{L} - [Ni]_0 - [Mn]_0 - [Co]_0\right)[1 - e^{(-k_1 t' + f)}] \quad (17b)$$

The parameters k_1 and f are gathered in **Table 6**.

The concentrations of lithium, nickel, cobalt and manganese dissolved at the transition time at the end of the first step can be calculated provided that the transition time has been calculated by using the preceding approach:

$$[Li]' = [Li] - [Li]_0 \quad (18)$$

$$[Ni]' = [Ni] - [Ni]_0 \quad (19)$$

$$[Mn]' = [Mn] - [Mn]_0 \quad (20)$$

$$[Co]' = [Co] - [Co]_0 \quad (21)$$

where $[Li]_0$, $[Ni]_0$, $[Mn]_0$ and $[Co]_0$ denote the concentration of lithium, nickel, manganese and cobalt at the end of the first step (at the transition time, see previously), respectively, whereas [Li]', [Ni]', [Mn]' and [Co]' represent nickel, cobalt, manganese and lithium concentrations dissolved in the leach solution during the second step, respectively.

According to **Eq (4)**, the following equation can be written:

$$[Ni]' + [Mn]' + [Co]' = n[Li]' = \frac{[HCl]_0 - [HCl]}{4} \quad (22)$$

According to the first-order rate law, the kinetics of HCl consumption during the second step can be described as follows:

$$[HCl] = [HCl]_f + \left([HCl]_0 - [HCl]_f\right)e^{-k_1 t'} \quad (23)$$

where [HCl] is the acid concentration at time t'=t-t_0 (time in the second step), $[HCl]_0$ is the acid concentration at the transition time t_0 and $[HCl]_f$ is the final acid concentration after full NMC dissolution. The model is appropriate to follow metal dissolution through acid consumption. Therefore, the combination of **Eqs (4), (22) and (23)** leads to the following relationship:

$$[Ni]' + [Mn]' + [Co]' = n[Li]' = \left(\frac{1}{M_{NMC}}\frac{S}{L} - [Ni]_0 - [Mn]_0 - [Co]_0\right)(1 - e^{-k_1 t'}) \quad (24)$$

Figure 10 shows that the first-order rate law can be used to describe the leaching kinetics of the second step given that a good agreement was obtained between the experimental data and

the values calculated by using **Eq (24)** [the same accordance was obtained for all leaching tests as shown in **Figure 11.**

3.1.3 Shrinking core model

Figure 1 shows that the particule size distribution is narrow in in the case of NMC811, and the same distribution was observed for all investigated cathodic materials. The SEM images of NMC811 after 5 minutes of leaching at 25 °C and abundant water washing, filtration and drying are reported in **Figure 12**. The initial spherical morphology of NMC was completly destroyed when 40% of lithium and 80% of nickel, manganese, and cobalt were dissolved. The overall leaching process may be controlled by intrinsic chemical reaction or by external mass transfer (diffusion). **Figure 12** shows the leaching process may not be controlled by ash diffusion as the particle size drastically decreased very early. It is more reasonable to consider the shrinking of small particles in Stokes regime, either film diffusion controls or reaction controls.

Therefore, the Shrinking Core model can be used to describe the leaching kinetics. In the shrinking core model, the function of the reaction conversion $f(x_i)$ of element i (i=Li, Ni, Mn and Co) is proportional to the reaction time t. The function $f(x_i)$ depends on the mechanism of the reaction (Liddell, 2005). The ratio of $f(x_i)$ over the reaction time t is called the reaction rate constant. In the case of the dissolution of several elements, each element i is characterized by its reaction rate constant $k_{R,i}$ in the case of chemical reaction control mechanism or its diffusion rate constant $k_{D,i}$ in the case of film diffusion control mechanism. Therefore, one of the following equations may describe the leaching kinetics (Levenspiel, 1999; Houzelot et al., 2018; Mgaidi et al., 2004):

In the case of chemical reaction control:

$$1-(1-x_i)^{\frac{1}{3}} = \left(\frac{3\beta_{r,i}[HCl]}{\rho_B R_0}\right) = k_{R,i}t \qquad (25)$$

In the case of film diffusion control:

$$x_i = \left(\frac{3\beta_{l,i}[HCl]}{\rho_B R_0}\right) = k_{D,i}t \qquad (26)$$

where x_i is the extraction fraction of the element i=Li, Ni, Mn or Co, and [HCl] represents the hydrochloric acid concentration in the bulk (the variation of hydrochloric acid in the bulk throughout the leaching experiments can be considered constant as shown previously). The parameters $\beta_{L,i}$, ρ_B, R_0 and $\beta_{r,i}$ denote the liquid mass transfer coefficient, the density of solid (in g cm^{-3}), the initial radius of the core (in cm) and the intrinsic chemical reaction rate constant, respectively. The terms $k_{R,i}$ and $k_{D,i}$ are rate constants depending upon the leaching mechanism: $k_{R,i}$ (in min^{-1}) is the apparent rate constant of the surface chemical reaction for i, $k_{D,i}$ (in min^{-1}) is the apparent diffusion rate constant of i, and t is the leaching time in minutes.

Since the reaction takes place in two steps, it is difficult to analyse the global reaction directly by means of the shrinking core model. **Figure 13** shows that the plots of $f(x_i)$ vs. time in the case of chemical reaction control and in the case of film diffusion control do not pass through the origin (0, 0) when NMC111 is leached in 4 mol L^{-1} HCl at 54 °C (same observation for all leaching experiments). In order to investigate the second step, which is the limiting step and the longuest step, it is necessary to subtract the concentrations of lithium, nickel, cobalt and manganese dissolved during the first step.

The Shrinking Core Model described by **Eqs (25)** and **(26)** can be applied to the second step by plotting [Li]', [Ni]', [Mn]' and [Co]' as a function of $t' = t - t_0$, as is done with first-order rate law in the previous sub-chapter. For the sake of illustration, **Figure 14** shows the plot of the shrinking core model applied to the longest step during the NMC111 dissolution in 4 mol L^{-1} HCl at 54 °C, considering both reaction controls and diffusion controls.

The kinetic parameters deduced from **Eqs (25) and (26)** for the investigated NMC materials at different temperatures are reported in **Tables S1-S4** (Supporting Information). The R^2 coefficient corresponding to reaction control is often higher than the R^2 coefficient found for diffusion control. It is therefore reasonable to conclude that the kinetics of the second step is controlled by the chemical reaction.

3.1.4 The effect of temperature and residence time

The temperature dependance of rate constants is usually described by the Arrhenius equation:

$$k_i = A_i exp\left(-\frac{E_{a,i}}{RT}\right) \quad (27)$$

where k_i (in min^{-1}) is the rate constant of i=Li, Ni, Mn or Co ($k_i=k_{R,i}$ in the case of chemical reation control, $k_i=k_{D,i}$ in the case of film diffusion control, $k_i=k_{1,i}$ in the case of first-order rate law). The term A_i is the frequency factor of i (in min^{-1}), $E_{a,i}$ (in J mol^{-1}) is the apparent activation energy of I, R is the universal gas constant (8.314 J mol^{-1} K^{-1}), and T is the absolute temperature (in K).

Figure 15 shows the Arrhenius plots corresponding to nickel dissolution from NMC111 in 4 mol L^{-1} hydrochloric acid at 54 °C. **Table 7** gathers the values of activation energies for the dissolution of lithium, nickel, manganese and cobalt during the lixiviation of NMC811, NMC622, NMC532 and NMC111 by considering the first-order rate law, and the shrinking core model including both reaction control and film diffusion control. It is interesting to highlight that the activation energies are very similar for the three models (first-order rate law, shrinking core model by considering a chemical reaction control and shrinking core model by

considering a film dissolution control). According to the literature, activation energies around 20 kJ mol^{-1} usually correspond to diffusion-controlled leaching whereas values higher than 40 kJ mol^{-1} can be attributed to chemical reaction-controlled leaching (Reid et al., 2017). Therefore, the values of the activation energies confirm the previous conclusion, i.e. the second step of NMC leaching is controlled by the chemical reaction.

The following equation deduced by combining **Eq (25)** [shrinking core model, reaction controls] and **Eq (27)** [Arrhenius law] can be used to calculate the dissolution yield of each metal contained in NMC at any leaching time and any temperature during the second step:

$$x_i = 1 - \left[1 - e^{\left(ln(A_i) - \frac{E_{a,i}}{RT}\right)} t'\right]^3 \quad (28)$$

where A_i is the frequency factor of i=Li, Ni, Mn or Co (in min^{-1}) reported in **Table 8**. $E_{a,i}$ (in J mol^{-1}) is the apparent activation energy of i =Li, Ni, Mn or Co. R is the universal gas constant (8.314 J mol^{-1} K^{-1}), T is the absolute temperature (in K) and t' is the leaching time of the second step in minutes.

The time to achieve the full dissolution of i=nickel, cobalt, manganese or lithium in the second step can be calculated from **Eq (29)** according to the shrinking core model:

$$t'_{i,100\%} = e^{\left[\frac{E_{a,i}}{RT} - ln(A_i)\right]} \quad (29)$$

Obviously, the full digestion of NMC will be reached by considering the highest value of $t'_{i,100\%}$ among those calculated for i=Li, Ni, Mn and Co.

Likewise, the First-order rate law can be used to calculate the leaching duration for achieving the full digestion of NMC. The time to reach LE% of extraction efficiency during the second step ($t'_{i,LE}$) can be deduced from the the first-order law:

$$t' = \frac{-\ln(100\% - LE(i)\%)}{k_{1,i}} = \frac{-\ln(100\% - LE(i)\%)}{A_i exp\left(-\frac{E_{a,i}}{RT}\right)} \quad (30)$$

where LE(i) and $k_{1,i}$ are the leaching percentage of i (i=Li, or the sum of Ni, Mn and Co) and the first-order rate constant of i, respectively.

Table 10 gathers the values of the leaching time necessary to reach the full dissolution of lithium, cobalt, nickel and manganese by considering shrinking core model and the first order law in the case of NMC811 dissolution. The duration to complete the full dissolution of NMC622, NMC532 and NMC111 are reported in Table S5-S7 in the Supporting Information. These Tables show a good agreement between the two models. It is possible to determine the residence time needed to reach the full dissolution of NMC by taking into consideration the maximum time of dissolution between the two models and by multiplying this value by 1.1 in

order to take into account the first step, which usually represents less than 10% of the global leaching time (see **Table 9**).

Figure 16 shows the variation of the residence time as a function of the temperature. The leaching kinetics follow the following order when temperature is comprised between 25 °C and 90 °C: NMC811>NMC622>>NMC532~NMC111. At high temperature, the behavior of NMC811 becomes close to that of NMC622. This order is in accordance with the fact that nickel decreases the thermal stability and manganese improves the stability of NMC cathodic materials (Gong et al., 2017) because of differences in temperature-dependence of NMC leaching kinetics (**Table 7**).

4. Conclusions

Hydrochloric acid is efficient for leaching NMC811, NMC622, NMC532 and NMC111. The apparent rate constants were calculated for each NMC at different temperatures. At 54 °C, the digestion of NMC811 and NMC622 is faster than the dissolution of NMC532 and NMC111. This observation complies with the fact that nickel is usually expected to increase dissolution rate and manganese stabilises the NMC structure.

The solid-liquid ratio does not affect the leaching kinetics as far as the solid-liquid phase ratio does not exceed the stochiometric limit. The leaching mechanism of NMC involves two steps: the first step is a fast phase transformation leading to the formation of a new lithium-defficient phase. This is in agreement with the XRD patterns, which confirm the presence of a shift of the main peak at the beginning of the leaching reaction, without further shifts during the rest of the reaction (Xuan et al., 2019). This transition phase is afterward dissolved during the second step, which is the rate-limiting reaction. Three semi-empirical kinetic models (semi-empirical model based on chloride consumption, shrinking core model and a model based on the first-order law) have been successfully applied to describe the leaching time of the investigated NMC cathodic materials.

The shrinking core model and a model based on the first-order law confirm that the kinetic of the second step is controlled by a chemical reaction. Two equations derived from the shrinking core model and the first order law have been reported to calculate the time necessary to achieve the complete leaching of NMC cathodic materials at any temperatures. Such an equation can be used to assess the optimized residence time in the leaching reactor as a function of the temperature and solid composition during NMC digestion.

Acknowledgements

This work was supported by the French National Research Agency through the national program ‘Appel à Projet Générique 2018’ (ANR-18-CE08-0005-03) and the national program "Investissements d'avenir" with the reference ANR-10-LABX-21-RESSOURCES21. The authors acknowledge the European Union within the framework of the operational programme FEDER-FSE Lorraine et Massif des Vosges 2014-2020 for their contribution in funding the Hydroval and Hydrolab facilitities. The authors are grateful to Jérôme Marin for the chlorine analyses in the samples.

References

Barik, S.P., Prabaharan, G., Kumar, L., 2017. Leaching and separation of Co and Mn from electrode materials of spent lithium-ion batteries using hydrochloric acid: Laboratory and pilot scale study. Journal of Cleaner Production 147, 37–43. https://doi.org/10.1016/j.jclepro.2017.01.095

Billy, E., Joulié, M., Laucournet, R., Boulineau, A., De Vito, E., Meyer, D., 2018. Dissolution mechanisms of $LiNi_{1/3}Mn_{1/3}Co_{1/3}O_2$ positive electrode material from Lithium-Ion Batteries in acid solution. ACS Appl. Mater. Interfaces, 10, 16424−16435.

Boyden, A., Soo, V. K., Doolan, M., 2016. The Environmental Impacts of Recycling Portable Lithium-Ion Batteries. Procedia CIRP. 48, 188 – 193.

Chagnes, A., Pospiech, B., 2013. A brief review on hydrometallurgical technologies for recycling spent lithium-ion batteries. J Chem Technol Biotechnol. 88, 1191–1199.

Chagnes, A. Recent Advances in Hydrometallurgy for the Development of a Sustainable Production of Lithium-Ion Batteries. ALTA 2019 - Lithium processing conference, May 2019, Perth, Australia.

Chen, W-S., Ho H-J., 2018. Recovery of valuable metals from Lithium-Ion Batteries NMC cathode waste materials by hydrometallurgical methods. Metals, 8, 321.

Chu, W., Zhang, Y., Chen, X., Huang, Y., Cui, H., Wang, M., Wang, J., 2020. Synthesis of $LiNi_{0.6}Co_{0.2}Mn_{0.2}O_2$ from mixed cathode materials of spent lithium-ion batteries. Journal of Power Sources 449, 227567. https://doi.org/10.1016/j.jpowsour.2019.227567

Dhiman, S., Gupta, B., 2019. Partition studies on cobalt and recycling of valuable metals from waste Li-ion batteries via solvent extraction and chemical precipitation. Journal of Cleaner Production 225, 820–832. https://doi.org/10.1016/j.jclepro.2019.04.004

Gaines, L., 2018. Lithium-ion battery recycling processes: Research towards a sustainable course. Sustainable Materials and Technologies 17, e00068. https://doi.org/10.1016/j.susmat.2018.e00068

Gong, J., Wang, Q., Sun, J., 2017. Thermal analysis of nickel cobalt lithium manganese with varying nickel content used for lithium-ion batteries. Thermochimica Acta. 655, 176-180.

He, L.-P., Sun, S.-Y., Song, X.-F., Yu, J.-G., 2017. Leaching process for recovering valuable metals from the LiNi 1/3 Co 1/3 Mn 1/3 O 2 cathode of lithium-ion batteries. Waste Management 64, 171–181. https://doi.org/10.1016/j.wasman.2017.02.011

Houzelot, V., Ranc, B., Laubie, B., Simonnot, M.-O., 2018. Agromining of hyperaccumulator biomass: Study of leaching kinetics of extraction of nickel, magnesium, potassium, phosphorus, iron, and manganese from Alyssum murale ashes by sulfuric acid. Chemical engineering research & design 129, 1–11. https://doi.org/10.1016/j.cherd.2017.10.030

Levenspiel, O., 1999. Chemical Reaction Engineering, third ed. John Wiley & Sens, New York.

Mantuano, D. P., Dorella, G., Elias, R. C. A., Mansur, M. B., 2006. Analysis of a hydrometallurgical route to recover base metals from spent rechargeable batteries by liquid–liquid extraction with Cyanex 272. Journal of Power Sources, 159(2), 1510–1518.

Li, J., Li, X., Hu, Q., Wang, Z., Zheng, J., Wu, L., Zhang, L., 2009. Study of extraction and purification of Ni, Co and Mn from spent battery material. Hydrometallurgy 99, 7–12. https://doi.org/10.1016/j.hydromet.2009.05.018

Liu, T., Chen, J., Li, H., Li, K., 2020. An integrated process for the separation and recovery of valuable metals from the spent $LiNi_{0.5}Co_{0.2}Mn_{0.3}O_2$ cathode materials. Separation and Purification Technology 245, 116869. https://doi.org/10.1016/j.seppur.2020.116869

Lu, W., Wang, Z., Cao, H., Zheng, X., Jin, W., Zhang, Y., Sun, Z., 2018. A sustainable process for metal recycling from spent lithium-ion batteries using ammonium chloride. Waste Management 79, 545–553. https://doi.org/10.1016/j.wasman.2018.08.027

Meshram, P., Pandey, B.D., Mankhand, T.R., 2015. Hydrometallurgical processing of spent lithium ion batteries (LIBs) in the presence of a reducing agent with emphasis on kinetics of leaching. Chemical Engineering Journal 281, 418–427. https://doi.org/10.1016/j.cej.2015.06.071

Mgaidi, A., Jendoubi, F., Oulahna, D., El Maaoui, M., Dodds, J.A., 2004. Kinetics of the dissolution of sand into alkaline solutions: application of a modified shrinking core model. Hydrometallurgy 71, p.435-446. https://doi.org/10.1016/S0304-386X(03)00117-8

Ordoñez, J., Gago, E.J., Girard, A., 2016. Processes and technologies for the recycling and recovery of spent lithium-ion batteries. Renewable and Sustainable Energy Reviews. 60, 195–205.

Pagliaro, M., Meneguzzo, F., 2019. Lithium battery reusing and recycling: A circular economy insight. Heliyon. 5, e01866.

Reid, S., Tam, J., Yang, M., Azimi, G. Technospheric Mining of Rare Earth Elements from Bauxite Residue (Red Mud): Process Optimization, Kinetic Investigation, and Microwave Pretreatment. Sci. Rep. 2017, 7 (15252), 1–9. https://doi.org/10.1038/s41598- 017-15457-8

Sattar, R., Ilyas, S., Bhatti, H.N., Ghaffar, A., 2019. Resource recovery of critically-rare metals by hydrometallurgical recycling of spent lithium ion batteries. Separation and Purification Technology 209, 725–733. https://doi.org/10.1016/j.seppur.2018.09.019

Seeley, F.G., Crouse, D.J., 1966. Extraction of Metals from Chloride Solutions and Amines. J. Chem. Eng. Data 11, 424–429. https://doi.org/10.1021/je60030a043

Sieber, T., Ducke, J., Rietig, A., Langner T., Acker, J., 2019. Recovery of $Li(Ni_{0.33}Mn_{0.33}Co_{0.33})O_2$ from Lithium-Ion Battery cathodes: aspects of degradation. Nanomaterials. 9, 246.

Takacova, Z., Havlik, T., Kukurugya, F., Orac, D., 2016. Cobalt and lithium recovery from active mass of spent Li-ion batteries: Theoretical and experimental approach. Hydrometallurgy 163, 9–17. https://doi.org/10.1016/j.hydromet.2016.03.007.

Wang, R.-C., Lin, Y.-C., Wu, S.-H., 2009. A novel recovery process of metal values from the cathode active materials of the lithium-ion secondary batteries. Hydrometallurgy 99, 194–201. https://doi.org/10.1016/j.hydromet.2009.08.005

Xuan, W., Otsuki, A., Chagnes, A., 2019. Investigation of the leaching mechanism of NMC 811 (LiNi 0.8 Mn 0.1 Co 0.1 O 2) by hydrochloric acid for recycling lithium ion battery cathodes. RSC Adv. 9, 38612–38618. https://doi.org/10.1039/C9RA06686A

Zheng, R.-J., 2017 A closed-loop process for recycling $LiNi_xCo_yMn_{(1-x-y)}O_2$ from mixed cathode materials of lithium-ion batteries. Green Energy & Environment 2, 42-50.

Zhu, Z., Yoko, P., Cheng, C.Y., 2017. Recovery of cobalt and manganese from nickel laterite leach solutions containing chloride by solvent extraction using Cyphos IL 101. Hydrometallurgy 169, 213–218. https://doi.org/10.1016/j.hydromet.2017.02.002

Zhuang, L., Sun, C., Zhou, T., Li, H., Dai, A., 2019. Recovery of valuable metals from $LiNi_{0.5}Co_{0.2}Mn_{0.3}O_2$ cathode materials of spent Li-ion batteries using mild mixed acid as leachant. Waste Management 85, 175–185. https://doi.org/10.1016/j.wasman.2018.12.034

480 **TABLES**

481

482 **Table 1**: Composition of the main cathodic materials in LIBs.

Abbreviation	Chemical formula
LCO	$LiCoO_2$
LMO	$LiMn_2O_4$
LNO	$LiNiO_2$
LFP	$LiFePO_4$
NMC111	$LiNi_{1/3}Mn_{1/3}Co_{1/3}O_2$
NMC532	$LiNi_{0.5}Mn_{0.3}Ni_{0.2}O_2$
NMC622	$LiNi_{0.6}Mn_{0.2}Co_{0.2}O_2$
NMC811	$LiNi_{0.8}Mn_{0.1}Co_{0.1}O_2$

483

484

Table 2: Experimental conditions implemented to leach cathodic materials from LIBs.

Cathode	Leaching media			Experimental conditions				Reference
	Acid	Concentration (M)	Additive	Temperature (°C)	Solid/Liquid % solids	Solid/Liquid mass/volume (g/ml)	Time (h)	
NMC111	H_2SO_4	1		30	4% (w/w)			Billy et al., 2018
NMC111, LCO	H_2SO_4	2	10% H_2O_2	70		1/30	1.5	Chen and Ho, 2018
NMC111, LCO, LMO	HCl	4		80		1/50	1	Wang et al., 2009
Spent LIBs cathods	HCl	1.75		50	20% (w/v)		2	Barik et al., 2017
NMC532	H_2SO_4	2	3% (v/v) H_2O_2	60		1/20	1	Liu et al., 2020
LCO, LMO, LNO, NMC	H_2SO_4	2.5	3.3% (v/v) H_2O_2	90			2.5	Chu et al., 2020
NMC, LFP, LIBs cathodes	HCl	6	H_2O_2/M^{2+}= 2 (mole)	60		1/8	2	Li et al., 2009
Spent LIBs cathodes	HCl	4		80		1/50	1	Dhiman et al., 2019
NMC, LiCoO2	H_2SO_4	1	1% (v/v) H_2O_2	40		1/25	1	He et al., 2017
Spent LIBs cathodes	H_3PO_4 and citric acid	0.2-0.4		90		1/50	0.5	Zhuang et al., 2019
Spent LIBs cathodes	H_2SO_4	2	4% (v/v) H_2O_2	50		1/20	2	Sattar et al., 2019
Spent LIBs cathodes	H_2SO_4	1	0.075 M $NaHSO_3$	95		1/50	4	Meshram et al., 2015
NMC cathode scrap	H_2SO_4	2.5	0.8 M NH_4Cl	80		1/10	1	Lv et al., 2018
Mixture of NMC, LCO, LMO, and LFP	H_2SO_4	2.5	20% (v/v) H_2O_2	60		1/33	1	Zheng et al., 2017

(see the cathode composition in **Table 1**).

Table 3: Comparison between the composition of NMC cathodic materials based on assays of solids after digestion (Exp. for experimental) and leach liquors (Cal. for calculated).

NMC	Composition % (w/w)									
	Ni		Co		Li		Mn		O	
	Exp.	Cal.	Exp.	Cal.	Exp.	Cal.	Exp.	Cal.	Exp.	Cal.
811	48.3	48.3	5.65	6.06	7.19	7.13	5.56	5.65	33.3	32.9
622	36.1	36.3	11.8	12.2	7.33	7.16	11.0	11.3	33.7	33.0
532	30.1	30.4	11.9	12.2	7.27	7.19	16.6	17.1	34.1	33.1
111	19.7	20.3	19.2	20.4	7.24	7.20	18.3	19.0	35.5	33.2

Table 4: Calculated values of n based on **Eqs (3) and (4)**.

NMC	Temperature (°C)	S/L (g/L)	n
811	25	80	3.60
811	25	20	2.83
811	35	20	3.55
811	43	20	3.79
811	54	20	4.00
622	44	20	2.67
622	54	20	2.28
622	63	20	2.86
622	72	20	3.11
532	54	20	2.44
532	63	20	2.63
532	72	20	2.28
532	82	20	2.60
111	54	20	2.11
111	63	20	2.38
111	72	20	2.72
111	82	20	2.71

Table 5: Parameters used in **Eq (6)** to calculate chloride consumption during NMC leaching at various temperatures.

NMC	Temperature (°C)	a (min^{-1})	$[Cl^-]_0$ ($mol \cdot L^{-1}$)	$[Cl^-]_\infty$ ($mol \cdot L^{-1}$)	u	R^2
811	25	0.03	4.06	3.28	0.99	0.96
622	44	0.07	4.07	3.87	1.00	0.95
622	54	0.11	4.01	3.78	0.97	0.97
622	63	0.60	4.06	3.83	1.00	0.98
622	72	2.00	4.13	3.90	1.00	0.92
532	63	0.12	4.10	3.92	1.00	0.94
532	72	0.28	4.06	3.89	1.00	0.97
532	82	0.72	4.08	3.91	1.00	0.97
111	63	0.10	4.02	3.84	1.00	0.93
111	72	0.39	4.06	3.88	1.00	0.97
111	82	0.69	4.06	3.89	1.00	0.95

The values of u and R^2 deduced from **Eq (7)** give information about the quality of the fit.

Table 6: Determination of the empirical parameters for **Eq (17)**.

NMC	Temperature (°C)	k_1	f
811	25	0.02	-0.42
811	35	0.06	-0.44
811	43	0.15	-0.41
811	54	0.41	-0.47
622	44	0.06	-0.41
622	54	0.20	-0.13
622	63	0.47	-0.33
622	72	1.43	-0.21
532	54	0.04	-0.43
532	63	0.11	-0.45
532	72	0.16	-0.46
532	82	0.86	-0.29
111	54	0.04	-0.44
111	63	0.09	-0.44
111	72	0.25	-0.39
111	82	0.60	-0.36

Table 7: Activation energy ($E_{a,i}$) of i=Li, Ni, Mn and Co deduced from Eq (27)[1].

NMC	Activation Energy (kJ/mol)									
	First-order Rate Law		Shrinking Core Model Reaction Controls				Shrinking Core Model Diffusion Controls			
	Ni / Mn / Co	Li	Ni	Co	Li	Mn	Ni	Co	Li	Mn
811	82.2	72.7	85.3	84.5	87.3	84.5	87.9	87.3	79.5	87.0
622	101	94.8	103	104	95.0	102	95.8	95.6	93.7	95.6
532	96.5	111	102	103	90.5	103	98.6	99.4	95.5	99.2
111	99.5	96.8	101	100	103	101	97.5	97.2	97.4	97.7

Table 8: Neperian logarithm of the frequency factor of i (A_i in min^{-1}) calculated by considering that leaching occurs via chemical reaction control, deduced from **Eq (27)**.

NMC	ln(A_i)					
	First-order Rate Law		Shrinking Core Model Chemical Controls			
	Li	Ni / Mn / Co	Li	Ni	Mn	Co
811	25.7	29.3	29.9	29.1	28.8	28.8
622	33.8	35.4	32.1	35.1	34.7	35.4
532	37.3	32.3	28.9	33.0	33.5	33.5
111	32.2	33.2	33.1	32.4	32.5	32.1

[1] Leaching conditions of NMC: 4 mol L^{-1} HCl at S/L=20 g/L.

Table 9: Time to finish the first step t_0 and total time to finish the whole reaction t, and their proportion.

NMC	Temperature (°C)	t_0 (min)	Total t (min)	t_0/t
811	25	7.54	220	0.03
811	35	2.32	85.5	0.03
811	43	0.83	32.5	0.03
811	54	0.18	11.9	0.01
622	44	2.20	80.3	0.03
622	54	1.90	25.9	0.07
622	63	0.50	10.6	0.05
622	72	0.21	3.05	0.07
532	54	3.04	111	0.03
532	63	0.56	38.9	0.01
532	72	0.39	29.2	0.01
532	82	0.25	5.84	0.04
111	54	3.46	139	0.02
111	63	0.87	56.7	0.02
111	72	0.56	19.9	0.03
111	82	0.28	8.20	0.03

Table 10: Residence time of the whole leaching reaction.

Temperature (°C)	Leaching time (min) NMC811				
	Reaction controls				First order rate law
	Li	Ni	Mn	Co	Ni + Mn + Co
25	207	199	206	199	245
30	116	113	117	113	142
35	66.0	65.0	68.1	65.7	83.4
40	38.3	38.2	40.2	38.8	50.0
45	22.6	22.8	24.1	23.3	30.4
50	13.6	13.9	14.7	14.2	18.8
55	8.28	8.54	9.12	8.80	11.8
60	5.12	5.34	5.73	5.53	7.51
65	3.21	3.39	3.65	3.52	4.84
70	2.05	2.18	2.35	2.27	3.16
75	1.32	1.42	1.54	1.49	2.09
80	0.86	0.93	1.02	0.98	1.40
85	0.57	0.62	0.68	0.66	0.95
90	0.38	0.42	0.46	0.45	0.65

The residence time is calculated according to shrinking core model (reaction controls) for Li, Ni, Mn, Co and first-order rate law for the sum of Ni, Mn and Co, during the dissolution of NMC811 in 4 mol L^{-1} HCl (Solid over liquid phase ratio S/L=20 g/L).

FIGURES

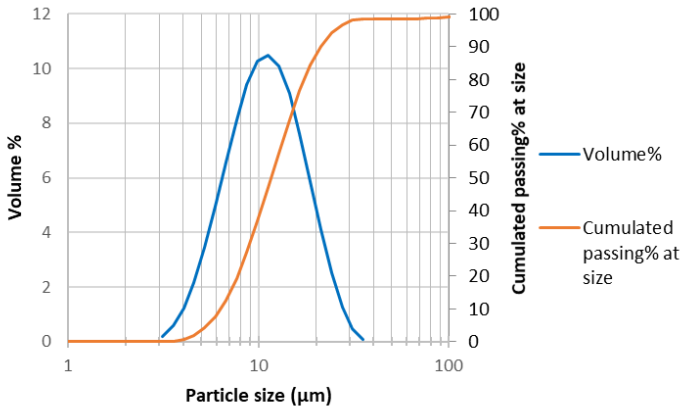

Figure 1: Particle size distribution of NMC811.

Figure 2: Setup for leaching experiments.

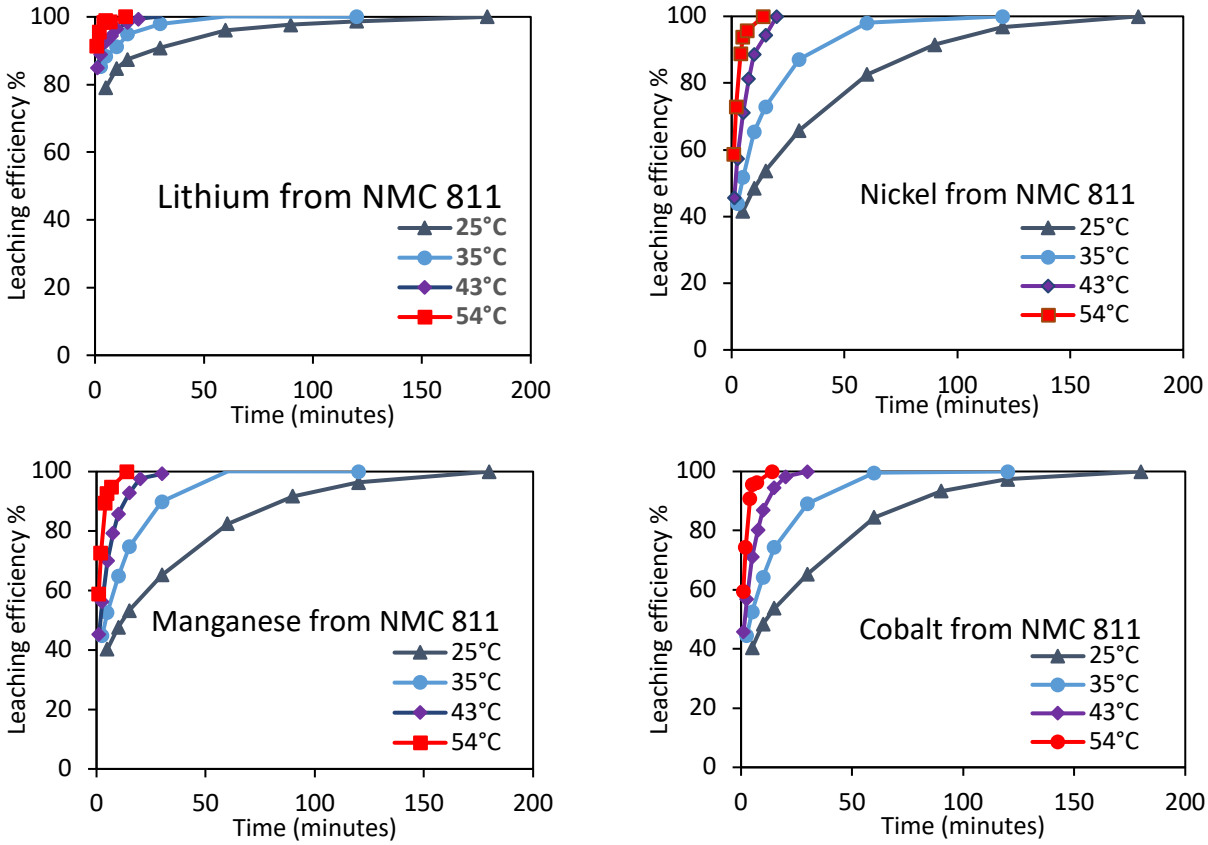

Figure 3: Dissolution kinetics of Li, Ni, Mn and Co from NMC811 in 4 mol L^{-1} HCl at 25 °C, 35 °C, 43 °C and 54 °C (Solid over Liquid phase ratio S/L=20 g/L).

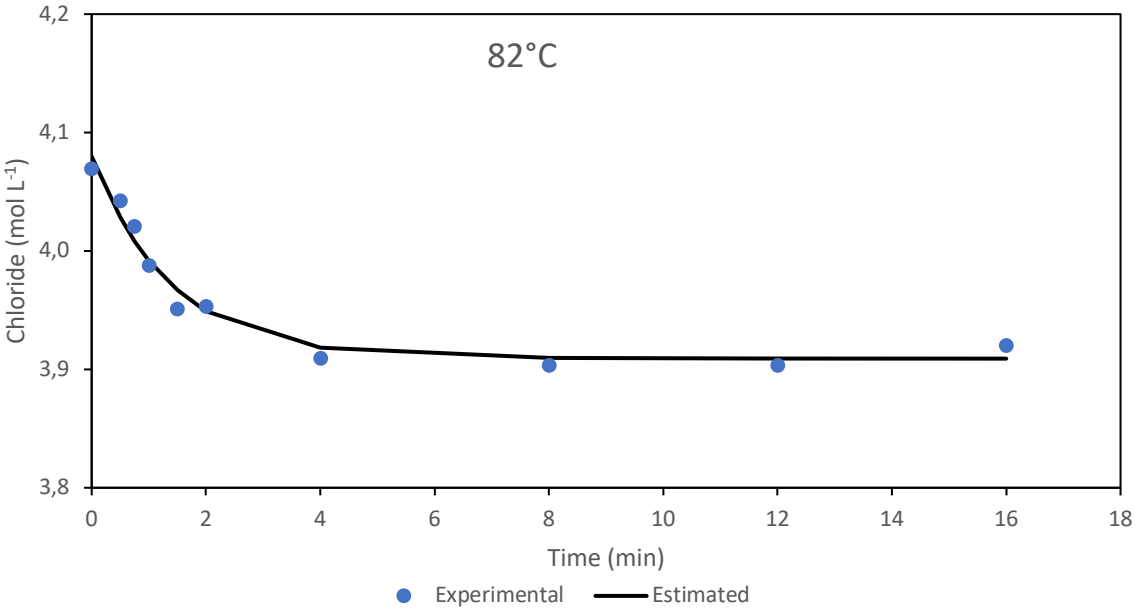

Figure 4: Chloride concentration in the leachate as a function of NMC532 leaching time in 4 mol L^{-1} HCl at 82 °C and S/L=20 g/L [see **Eq (6)**].

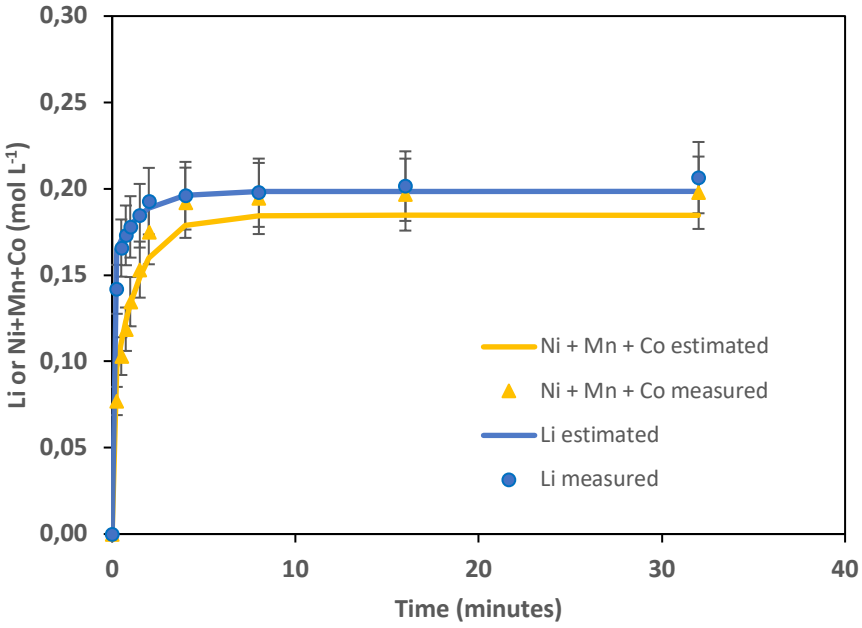

529

530 **Figure 5:** Li concentration and sum of the concentrations of Ni, Mn and Co in the leachate at
531 82 °C and S/L= 20 g/L during NMC532 leaching in 4 mol L^{-1} HCl. Calculations performed by
532 using **Eqs (9) and (10)**.

533

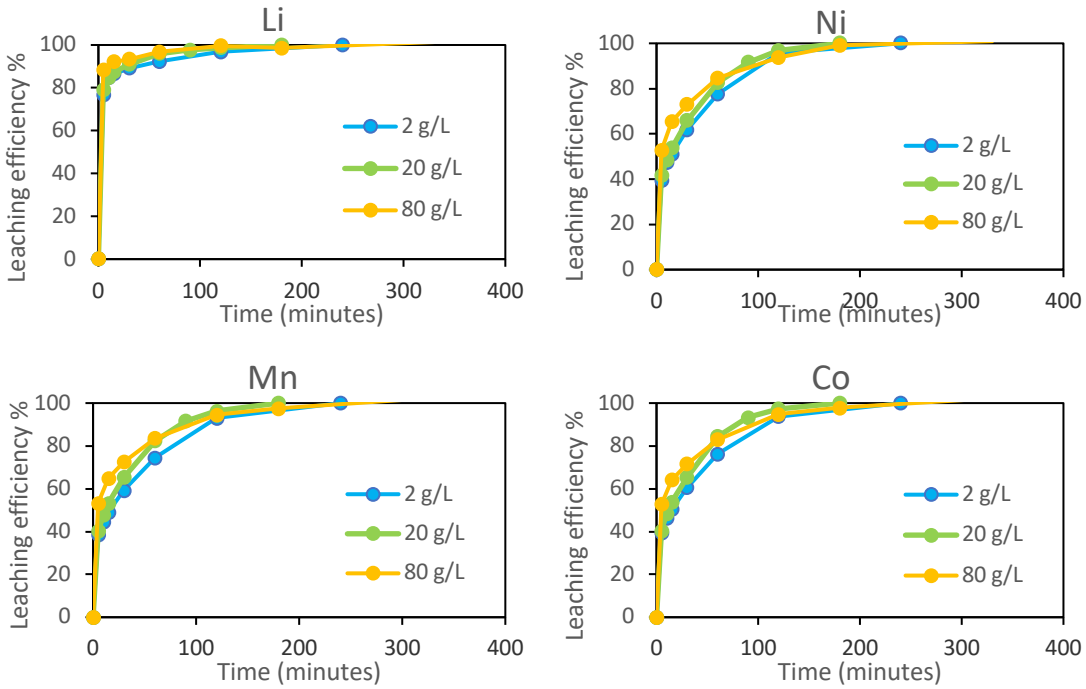

534

535

536 **Figure 6:** Effect of S/L on the leaching kinetics of NMC811 in 4 mol L^{-1} HCl at 25 °C.

537

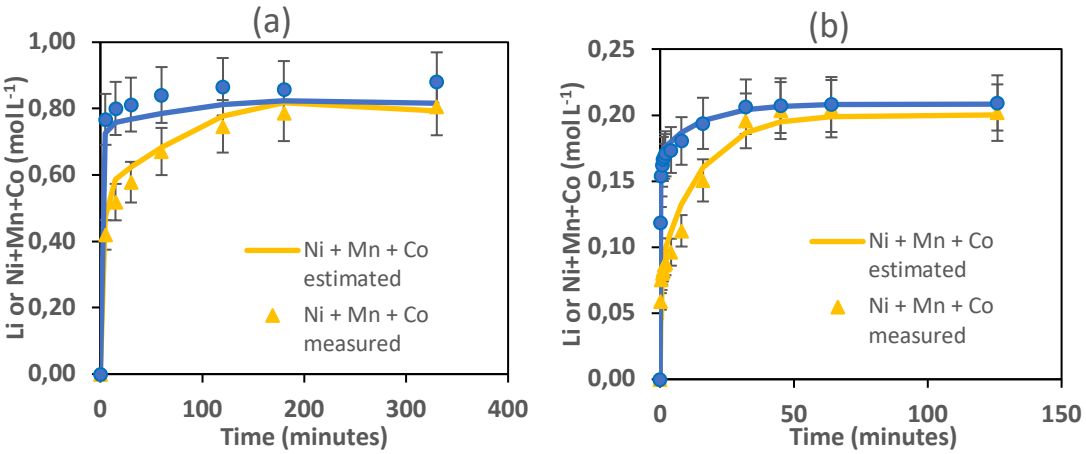

538

539 **Figure 7**: Lithium concentration and the sum of the concentrations of Ni, Mn and Co in the
540 leachate during (a) NMC 811 dissolution at 25 °C and S/L= 80 g/L, and (b) NMC622
541 dissolution at 54 °C and S/L= 20 g/L. Dissolution were performed in 4 mol L^{-1} HCl.
542 Calculations were performed by using **Eqs (9) and (10)**.

543

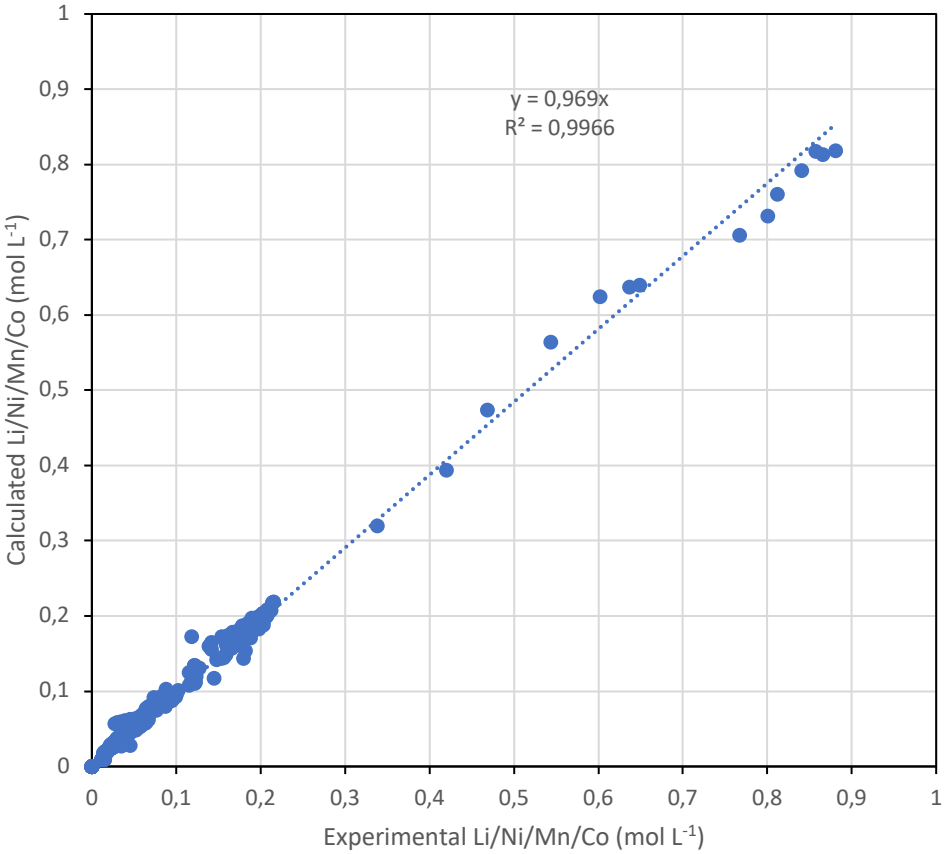

544

545 **Figure 8:** Comparison of the experimental and calculated concentrations of lithium, nickel,
546 cobalt and manganese in the leach solutions [see **Eqs (9) and (10)**].

547

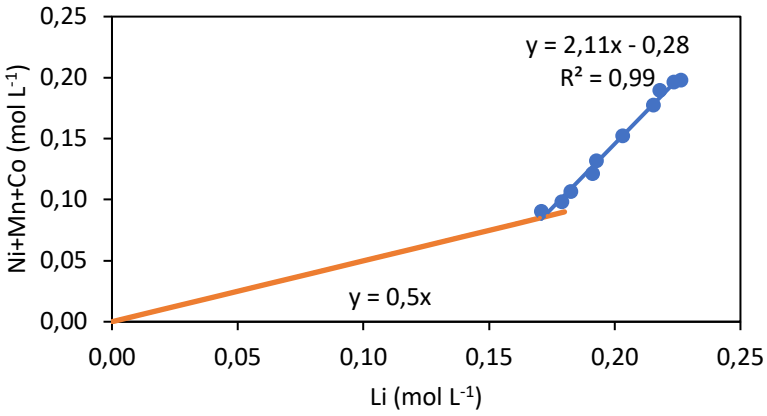

548

549 **Figure 9**: Determination of the transition point between step 1 (red cruve) and step 2 (blue
550 curve) during the NMC111 dissolution in 4 mol L^{-1} HCl at 54 °C.

551

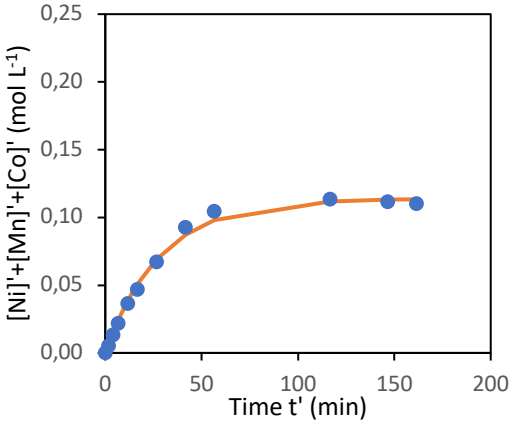

552

553 **Figure 10**: The sum of the concentrations of Ni, Mn and Co during the second step of NMC
554 111 dissolution at 54 °C and S/L= 20 g/L. The dissolution was performed in 4 mol·L^{-1} HCl.

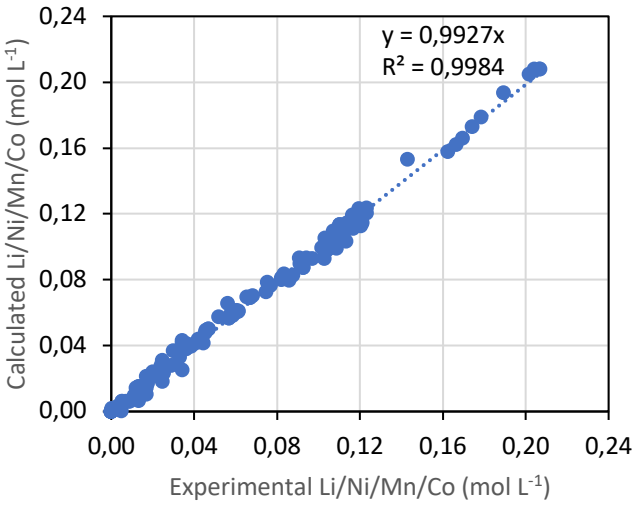

555

556 **Figure 11:** Comparison of the experimental and calculated concentrations of lithium, nickel,
557 cobalt and manganese in the leach solutions, generated during the second step.

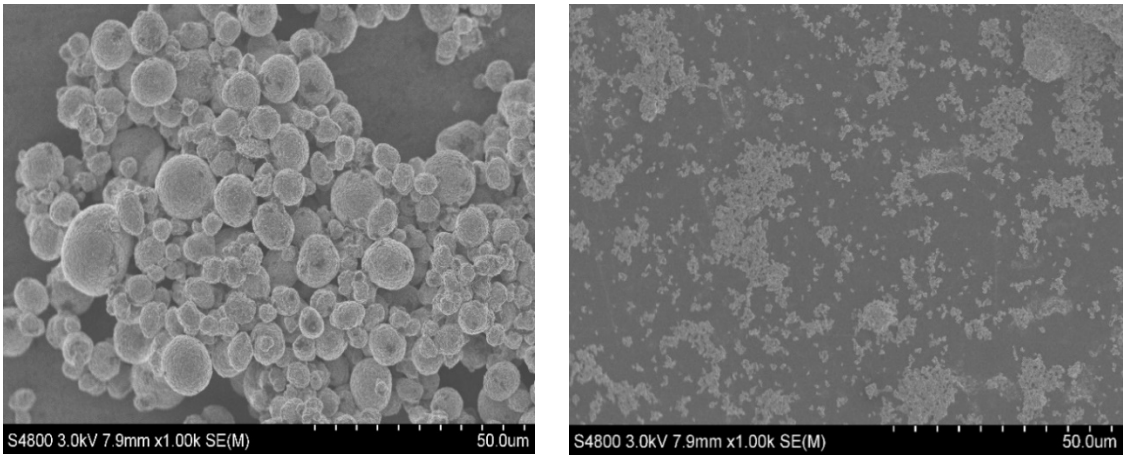

(a) (b)

Figure 12: SEM images of (a) the pristine NMC 811 cathodic material, (b) NMC811 withdrawn after 5 minutes of leaching in 4 mol L^{-1} HCl at S/L=2 g/L and 25 °C.

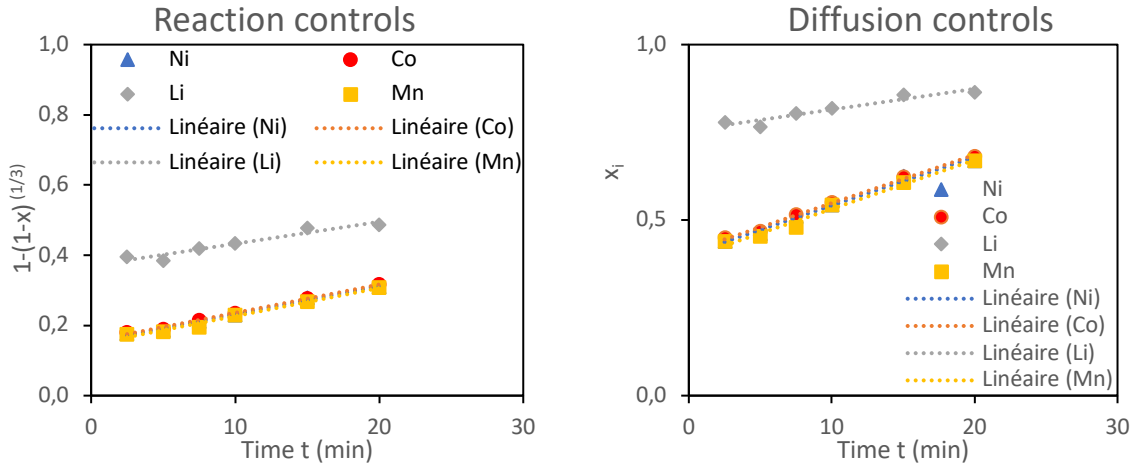

Figure 13: Application of shrinking core model to the global reaction of NMC 111 dissolution in 4 mol L^{-1} HCl at 54°C.

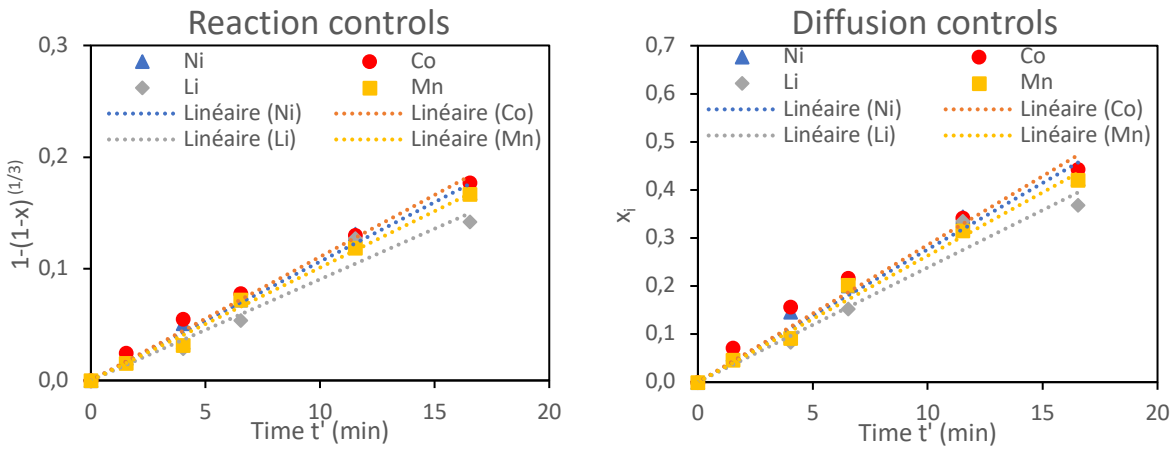

Figure 14: Application of the shrinking core model to the second step of NMC 111 dissolution in 4 mol L^{-1} HCl at 54°C.

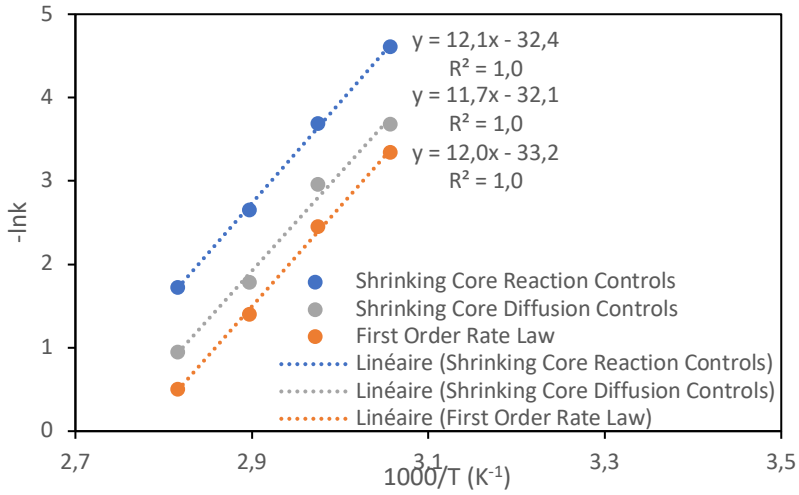

566 **Figure 15**: Arrhenius plots of Ni in the second step of NMC 111 dissolution in 4 mol L^{-1} HCl
567 at temperature range between 54 and 82°C according to **Eq (27)**.

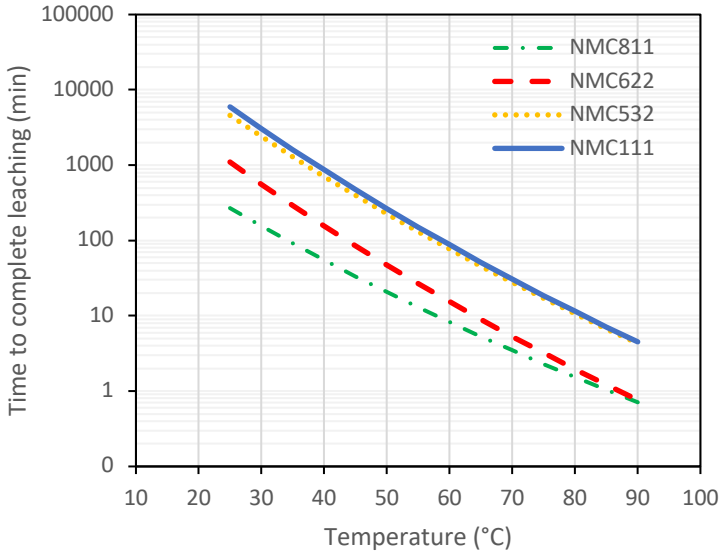

568

569 **Figure 16:** Leaching time to achieve the full dissolution of NMC materials in 4 mol L^{-1} HCl as
570 a function of the temperature at S/L= 20 g/L. The data were calculated by using **Eqs (29) and**
571 **(30)**.